Journal of
Applied Remote Sensing

RemoteSensing.SPIEDigitalLibrary.org

Mapping of peanut crops in Queensland, Australia, using time-series PROBA-V 100-m normalized difference vegetation index imagery

Haerani Haerani
Armando Apan
Badri Basnet

SPIE.

Haerani Haerani, Armando Apan, Badri Basnet, "Mapping of peanut crops in Queensland, Australia, using time-series PROBA-V 100-m normalized difference vegetation index imagery," *J. Appl. Remote Sens.* **12**(3), 036005 (2018), doi: 10.1117/1.JRS.12.036005.

Downloaded From: https://www.spiedigitallibrary.org/journals/Journal-of-Applied-Remote-Sensing on 7/24/2018
Terms of Use: https://www.spiedigitallibrary.org/terms-of-use

Mapping of peanut crops in Queensland, Australia, using time-series PROBA-V 100-m normalized difference vegetation index imagery

Haerani Haerani,[a,b,c,*] Armando Apan,[c,d] and Badri Basnet[c]

[a]University of Southern Queensland, International Centre for Applied Climate Sciences, Toowoomba, Australia

[b]Universitas Hasanuddin, Agricultural Engineering Department, Makassar, Indonesia

[c]University of Southern Queensland, School of Civil Engineering and Surveying, Toowoomba, Australia

[d]University of Southern Queensland, Institute for Agriculture and the Environment, Toowoomba, Australia

Abstract. Mapping of peanut crops is essential in supporting peanut production, yield prediction, and commodity forecasting. While ground-based surveys can be used over small areas, the development of remote-sensing technologies could provide rapid and inexpensive crop area estimates with high accuracy over large regions. Some of these recent earth observation satellite systems, such as the Project for On-Board Autonomy Vegetation (PROBA-V), have the advantage of increased spatial and temporal resolution. With a study area located in the South Burnett region, Queensland, Australia, the primary aim of this study was to assess the ability of time-series PROBA-V 100-m normalized difference vegetation index (NDVI) for peanut crop mapping. Two datasets, i.e., PROBA-V NDVI time-series imagery and the corresponding phenological parameters generated from TIMESAT data analysis technique, were classified using maximum likelihood classification, spectral angle mapper, and minimum distance classification algorithms. The results show that among all methods used, the application of MLC in PROBA-V NDVI time series produced very good overall accuracy, i.e., 92.75%, with producer and user accuracy of each class ≥78.79%. For all algorithms tested, the mapping of peanut cropping areas produced satisfactory classification results, i.e., 75.95% to 100%. Our study confirmed that the use of finer resolution 100 m of PROBA-V imagery (i.e., relative to MODIS 250-m data) has contributed to the success of mapping peanut and other crops in the study area. © *2018 Society of Photo-Optical Instrumentation Engineers (SPIE)* [DOI: 10.1117/1.JRS.12.036005]

Keywords: Project for On-Board Autonomy Vegetation; normalized difference vegetation index; time series; mapping; peanuts; classification.

Paper 180217 received Mar. 15, 2018; accepted for publication Jun. 12, 2018; published online Jul. 12, 2018.

1 Introduction

Peanut or groundnut (*Arachis hypogea* L.) is one of the most important legume crops, as it is an important source of protein and oil,[1] and it has 26% protein higher than eggs, dairy products, meat, and fish.[2] Generally, peanut-growing countries use their production output to meet their domestic market.[2] In Australia, peanut production is about 40,000 tons per year, which is <0.2% of the world's peanut production. The crop area planted in Australia is about 15,000 ha, and more than 90% is located in Queensland.[3] In Queensland, the peanut industry contributed to gross value production of 15.2 million dollars in 2014/2015.[4] In general, Australian peanut production can meet domestic demand, except when a severe drought occurs. However, efforts

*Address all correspondence to: Haerani Haerani, E-mail: haerani.-@usq.edu.au, haerani@agri.unhas.ac.id

1931-3195/2018/$25.00 © 2018 SPIE

Downloaded From: https://www.spiedigitallibrary.org/journals/Journal-of-Applied-Remote-Sensing on 7/24/2018
Terms of Use: https://www.spiedigitallibrary.org/terms-of-use

have been made to develop and supply an export market.[2] Therefore, there is a need to increase the industry's capabilities in producing peanut using more effective and efficient methods to meet production demands and profitability.

Crop area estimation and crop yield estimation are the two main components of crop production.[5,6] Compared to crop area estimation, more studies have been conducted on crop yield estimation.[6,7] For years, crop area estimation has been collected by censuses, which is accurate but expensive and time consuming, or by samples, which is cheap but not always accurate.[6] Remote sensing offers great help in crop area estimation by providing opportunities to increase the accuracy of the estimate and to reduce associated time and cost of mapping. It has distinct benefits pertaining to rapid objective assessment and longitudinal assessment, i.e., capturing changes over time at the same area.[8] Utilizing remote sensing may allow crop area estimates to be conducted several months before harvest, including in the early season. This will be beneficial in making decisions such as supply, staff requirements, and import needs.[9] However, studies on peanut crop mapping using satellite imagery are limited.

Schultz et al.[10] studied crop mapping of several crops, including peanut, in a subtropical region, Brazil, using Landsat imagery and employing a combination of segmentation and random forest (RF) classification algorithm. It was found that using Landsat imagery is not enough to separate peanut and cassava due to similarity in spectral behavior and the high variabilities within the class. In Australia, Robson et al.[9] employed a single-date high-resolution QuickBird imagery in one area of the South Burnett to identify spatial variability in peanut fields. This study also mapped peanut crops within the area with accurate results. However, this study was conducted in small areas (64 km^2) and used a high spatial resolution satellite imagery. In Senegal, a study on peanut crop yield estimation has been done in a peanut-growing region (peanut basin),[11] but peanut crop area mapping has not been conducted.

Crop mapping using satellite imagery can be done using multispectral, radar, and hyperspectral sensors. Having many narrow spectral bands, hyperspectral satellite data provide the opportunity to collect more detailed spectral information than the few broad spectral bands of multispectral sensors.[12] Therefore, hyperspectral data can adequately discriminate crops' properties and can perform well in crop mapping.[13] Nevertheless, fewer hyperspectral sensors are mounted in satellites (i.e., Hyperion EO-1),[14] which results in limited data availability. In regard to multispectral sensors, it is often difficult to classify different crop types using a single image,[15] since crops frequently demonstrate very similar spectral behavior.[16] However, different physiological growth phases of each crop exhibit different spectral behavior; thus, the use of multispectral time-series imagery provides an opportunity to capture these temporal differences.[16] This intra-annual multispectral time-series imagery can produce average phenology of individual land cover types,[17] which is an indirect estimation of physiological crop growth phases.[18] As a result, crops with similar spectral behavior can be classified easily using this time-series data.[16] In a study of crop classification in Kansas, the VI time-series profile of a crop was found to be similar with its phenology attributes, such as timing of green-up, peak greenness, and senescence.[19]

Several mathematical functions have been used to smooth time-series vegetation indices from various satellite sensors.[20,21] These include principal component analysis,[22] harmonic analysis,[23] harmonic analysis of time series,[24] Savitzky–Golay filter,[25] double logistic function fitting,[26] and asymmetric Gaussian function fitting.[27] Some tools have been developed to analyze time-series data, such as TIMESAT, TIMESTATS, TiSeG, BFAST, and STARFM.[28] TIMESAT is a free software program that uses a curve fitting approach to smooth noisy time-series imagery to generate phenological parameters and map them.[27,29,30] Using phenological parameters of MODIS enhanced vegetation index imagery produced from the TIMESAT program, Yang et al.[31] successfully mapped paddy rice in China. However, the use of a TIMESAT program in mapping land use and land cover in a semihumid tropical region of Zimbabwe using time-series MODIS has failed to distinguish rainfed agriculture from grassland.[32]

Mapping agricultural land use requires the consideration of spatial resolution, temporal resolution, coverage, availability/quality (such as cloud cover), imagery costs, and classification methods.[33] The definition of spatial resolution of satellite imagery may be divided into four:[34] (1) coarse- or low-resolution imagery has a ground sampling distance (GSD) $\geq$30 m; (2) medium resolution is defined as resolution with a GSD between 2 and 30 m; (3) high-resolution imagery has a GSD in the range of 0.5 to 2.0 m; and (4) very high resolution

Downloaded From: https://www.spiedigitallibrary.org/journals/Journal-of-Applied-Remote-Sensing on 7/24/2018
Terms of Use: https://www.spiedigitallibrary.org/terms-of-use

has a GSD <0.5 m. Fundamentally, the trade-off in mapping crops is focused on temporal versus spatial resolutions.[35] Higher-resolution (high spatial) data provide an opportunity to capture in-depth local information,[33,36] which is appropriate to map cropping areas on a small scale.[37] The use of decametric sensors, such as Landsat (30 m), ASTER (15 m), Sentinel-2 (10 m), and Resourcesat-2 (5.8 m), will be useful in mapping crop areas with paddocks of a few hectares.[10] However, most of these sensors usually have insufficient temporal resolution to generate crop phenology stages,[38] e.g., Landsat and ASTER have a temporal resolution of 16 days. Another disadvantage of using these sensors is the possibility of having noise, due to cloud cover.[39] Coarse-resolution (low spatial) sensors, e.g., MODIS (250 m), AVHRR (1 km), and SPOT-Vegetation (1 km), have become the main sources of data for mapping large areas, for example in the United States.[40] These sensors typically have wider swaths, which lead to high temporal resolution data;[35] for example, MODIS and AVHRR have a resolution of 1 to 2 days and <1 day, respectively. Nevertheless, in mapping small paddock sizes, inaccurate estimates may result from these sensors due to their coarse spatial resolution.[35] To compensate for the trade-off, some studies composite imagery data using different sensors; for example, Liu et al.[41] incorporated high and low spatial resolution image in their crop mapping study. Nevertheless, with their frequent temporal resolution, coarse-resolution sensors are more feasible to get cloud-free imagery and are suitable for gaining time-series data,[33,36] which can facilitate the derivation of phenology phases.[38]

Many agricultural fields are characterized by small farm size (i.e., <1 ha). Thus, to accurately map crops, a medium-to-high spatial resolution imagery, with a pixel size of 5 to 100 m, is required.[41] A recent earth observation satellite, namely Project for On-Board Autonomy Vegetation (PROBA-V), could satisfy this requirement, since it has a spatial resolution of 100 m. Moreover, derived normalized difference vegetation index (NDVI) products are also available from PROBA-V,[42] which could be very useful in mapping crops. This satellite has finer spatial resolution than the commonly used coarse-resolution satellite data, i.e., MODIS, which has 250-m resolution, although both satellites have similar temporal resolution, i.e., daily (PROBA-V) and 1 to 2 days (MODIS). The increasing resolution of PROBA-V can potentially generate better accuracy, since the number of spectral mixtures can be eliminated.[43] For instance, Zhang et al.[39] compared the use of MODIS and PROBA-V to map crops in complex cropping systems in Hongxing, China, and revealed that PROBA-V generated better accuracy (73.29%) compared to MODIS (46.81%). In addition, crop mapping studies using PROBA-V imagery are limited since this remote-sensing satellite was launched in recent years.[44] For instance, Lambert et al.[45] have recently mapped cropland in Sahelian and Sudanian regions using 100-m PROBA-V time series. Moreover, the successful study of crop area mapping with PROBA-V in Belgium, Russia, Ukraine, and Brazil provides the possibility of using this remote-sensing system to map crop areas around different regions in the world.[44] Thus, the use of PROBA-V time-series satellite imagery in mapping peanut crops over regional areas in Australia has been examined in this study.

The primary aim of this study was to assess the effectiveness of time-series PROBA-V 100-m NDVI imagery for peanut crop mapping in the South Burnett region of Queensland, Australia. The following are the specific objectives: (1) to map peanut crops using PROBA-V 100-m NDVI images and test the value of crop phenology as an alternative to traditional approach and (2) to determine the most appropriate classification method(s) in mapping peanut crops in the study area. This study attempted to contribute knowledge on the application of a relatively finer (100 m) remote-sensing data product, including the assessment of multitemporal data analysis techniques, to peanut crop mapping and monitoring. This is particularly true for mapping crops during the summer season where cloud cover is a major issue.

2 Materials and Methods

2.1 *Study Area*

The region selected for this study is located in the South Burnett region, Queensland, Australia, covering an area of 8381.70 km^2 (Fig. 1).[46] The climate in the study site is temperate,[47] with the

Downloaded From: https://www.spiedigitallibrary.org/journals/Journal-of-Applied-Remote-Sensing on 7/24/2018
Terms of Use: https://www.spiedigitallibrary.org/terms-of-use

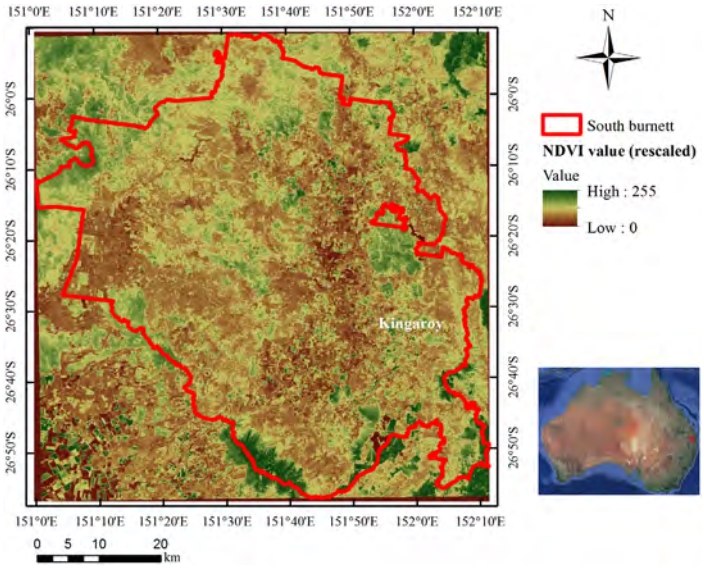

Fig. 1 Study area in the South Burnett region, Queensland.

average mean maximum temperature between 19.4°C in July and 30.8°C in January, while the average minimum temperature is between 3.4°C in July and 18.0°C in January.[48] It falls within the summer rainfall zones,[47] with mean annual rainfall of 662.6 mm, while the wettest month (108.1 mm) is recorded in December.[48] These temperature and rainfall ranges are suited for peanut crops, i.e., 25°C to 30°C during vegetative growth and 22°C to 24°C during generative growth, with 500 to 600 mm well distributed rainfall.[2] The region has a soil dominated by red ferrosols, which is suitable for growing peanut crops.[49] Summer and winter crops, such as peanuts, navy bean, wheat, and sorghum, are often planted in this region.[50] These summer crops are typically sowed in September to early January and usually harvested in February to May.[51]

2.2 *Image Data Acquisition and Preprocessing*

PROBA-V offers an intermediary spatial resolution between medium spatial resolution imagery, such as Landsat and HJ-1 A/B (30-m resolution), and low spatial resolution datasets, such as MODIS, SPOT-Vegetation, and AVHRR (250-m to 1-km resolution).[39] It was specifically designed as a "gap-filler mission" between SPOT-Vegetation, which was terminated in 2014, and ESA Sentinel-3 satellite, to ensure the continuation of vegetation time-series data.[52,53] The end-user products include daily synthesis (S1) collections, which are available for

Table 1 Summary of imagery used in this study.

Imagery	Characteristics
Product	End-user product (level 3) of S1TOC NDVI
Spatial resolution	100 m
Swath	517 km
Global coverage	5 days
Date/period	June 3, 2015, to June 28, 2016
Number of imagery	24 cloud-free imagery
Tile	X33Y10
File format	HDF5

Downloaded From: https://www.spiedigitallibrary.org/journals/Journal-of-Applied-Remote-Sensing on 7/24/2018
Terms of Use: https://www.spiedigitallibrary.org/terms-of-use

100-m, 300-m, and 1-km resolution, and 5-day synthesis (S5) with 100-m resolution top-of-atmosphere reflectance. In addition, top-of-canopy (TOC) (atmospherically corrected) products are also available, including a 10-day synthesis (S10) with 300-m and 1-km resolution. NDVI collections are available for S1 and S5 products with 100-m resolution, as well as S10 datasets with 300-m and 1-km resolution TOC.

In this study, PROBA-V S1TOC (daily synthesis atmospherically corrected) 100-m NDVI products were selected in mapping peanut crops (Table 1). Since the growing season of peanut crops in this region is between October and June, images were collected during the period of June 2015 to June 2016 to adequately cover the entire season. A total of 163 images covering the study area from X33Y10 PROBA-V tile were available. However, only cloud-free images were selected and processed for this study, which resulted in 24 images. A coverage of one-year time-series data was used, since multiple years' data can generate inaccurate phenological features[54] and may cause confusion due to land cover changes.[18] Afterward, the 24 images were subset into a study area and reprojected into a Universal Transverse Mercator projection. Last, the original NDVI values for each image were rescaled (0 to 255) using a linear function to enable software compatibility, better data handling, and data standardization.

2.3 *Field Data Gathering*

In March 2016, a field survey of various locations throughout the study area was conducted to collect training areas or region of interest (ROI) for classification and accuracy assessment. Using a Global Positioning System, the reference data collection was conducted by capturing crops or land feature types (i.e., peanut, corn, sorghum, mung bean, woody vegetation, pasture, and water) on the main, secondary, and farm roads. It was done by randomly selecting large paddocks, water bodies, pasture lands, and forest vegetation areas to avoid mixed pixels, and ensuring geographical representativeness of the reference data. In addition, high-resolution images from Landsat 8 satellite captured on March 25, 2016, and from Google Earth captured in March 2015 were also used to determine ROIs using visual interpretation techniques.[55] Typical appearances of crop classes examined in this study taken from TIMESAT output of crop phenology, a Landsat image, and field work photos were shown in Fig. 2. Based on study area observation during the field work, there were eight[8] classes selected for this study with a total number of reference data of 1690 pixels (Table 2). The original pixel size of 100×100 m was retained for the training samples.

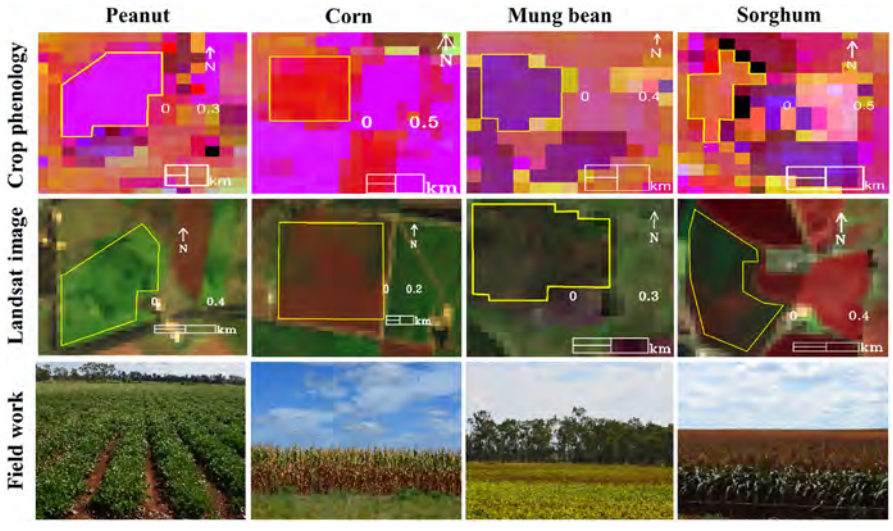

Fig. 2 Example images of peanut, corn, mung bean, and sorghum classes were taken from crop phenology layers of TIMESAT program, a Landsat image, and field work photos. The yellow lines indicate the boundary of paddocks for each class. The Landsat image, particularly corn, may not represent the actual cover due to the date of data captured (i.e., during harvesting time).

Downloaded From: https://www.spiedigitallibrary.org/journals/Journal-of-Applied-Remote-Sensing on 7/24/2018
Terms of Use: https://www.spiedigitallibrary.org/terms-of-use

Table 2 Total number of reference data for each class.

Class	Training data
Peanut	263
Mung bean	63
Corn	198
Sorghum	63
Pasture	368
Bare soil	161
Woody vegetation	412
Water	162
Total	1690

2.4 *Extracting Time-Series Profiles and Separability Test*

The time-series profiles of NDVI datasets were generated and displayed by extracting the average spectral value of selected sample pixels from each date/layer of 24 NDVI image data for each class. Field data and high-resolution image from Google Earth were used as references in determining pixel samples, where only "pure pixels" were selected. Pure pixels ensure that the chosen pixels were indeed the pixels of the representative class. In this case, pixels in the middle of paddock or class area were chosen. Spectral profiles were used to observe the reflectance pattern and differences between classes, including the examination of temporal separability. Especially for crop classes, such profiles were also used to examine the ability of PROBA-V NDVI imagery in presenting crop phenology cycles and aging.[56] In addition, a separability test, namely Jeffries–Matusita (JM) distance, was performed to avoid or reduce potential misclassification due to using similar classes in classification.[57] Beyer et al.[16] have demonstrated the effectiveness of JM as a pretesting method in finding the best layer stack combination for spectral separation of different land cover classes. This test can be used to determine the spectral distance between any pair of layers before conducting classification. If the distance is insignificant, the layers can be eliminated from the classification to ensure the best result.[58] JM distance measures the separability between a pair of two classes based on the average distance between their spectral means. Its output value ranges from 0 to 2, where a good separability is indicated by a larger value.[19] The JM distance between a pair of probability distributions is calculated as

$$J_{ij} = \int_x \left[\sqrt{p(x/\omega_i)} - \sqrt{p(x/\omega_j)}\right]^2 \mathrm{d}x. \tag{1}$$

In this study, x represents the span of NDVI time-series values, while i and j represent crop and/or other land cover classes under consideration. In a normally distributed assumption, Eq. (1) becomes

$$J_{ij} = 2(1 - e^{-B}), \tag{2}$$

where

$$B = 1/8D^2 + 1/2 \ln\left[\left(\left|\sum i + \sum j\right|2\right)/\left(\left|\sum i\right|^{1/2}\left|\sum j\right|^{1/2}\right)\right] \tag{3}$$

and

$$D^2 = (m_i - m_j)^t\left[\left(\sum i + \sum j\right)/2\right]^{-1}(m_i - m_j). \tag{4}$$

Downloaded From: https://www.spiedigitallibrary.org/journals/Journal-of-Applied-Remote-Sensing on 7/24/2018
Terms of Use: https://www.spiedigitallibrary.org/terms-of-use

2.5 *Time-Series Image Analysis*

PROBA-V NDVI imagery was used to map peanut crops, other crops, and additional land cover classes by stacking the 24 image data and generating phenological parameters imagery using a TIMESAT software program.[27,29] The entire workflow to map these land cover features is shown in Fig. 3. TIMESAT analyzes time-series data in relation to its seasonality, such as phenology and temporal development.[30] It is a user-friendly software with advanced algorithms.[59] The program generates 11 phenological parameters of a growing season, such as start and end seasons (Table 3 and Fig. 4).[30]

The TIMESAT program iteratively fits mathematical functions to smooth noisy time-series data, in which the phenological parameters are extracted from each imagery pixel.[60] Theoretically, as long as the growing season peaks in the middle of a year, the phenological parameters could be generated from each year of time-series data. However, TIMESAT is not based on this. In TIMESAT, for a time-series spanning n years, the number of years of phenological parameters produced will be $n - 1$ center-most seasons.[30] Therefore, for one-year time-series data, i.e., the case for our study, Eklundh and Jönsson[30] recommend the creation of artificial time-series data for the dataset of first and third years, since the phenological parameters will be calculated from the center of time-series data, i.e., our original year data. The artificial time-series data were created by duplicating our one-year time-series data.

Three fitting methods to the upper envelope of time-series data are available in the TIMESAT program, i.e., Savitzky–Golay filter, asymmetric Gaussian, and double logistic.[29] In this study, the asymmetric Gaussian (local polynomial function) was used, since this method is less sensitive to time-series noise and provides better results for the season start and season end parameters.[29] The TIMESAT program comprises various processing aspects, such as choosing

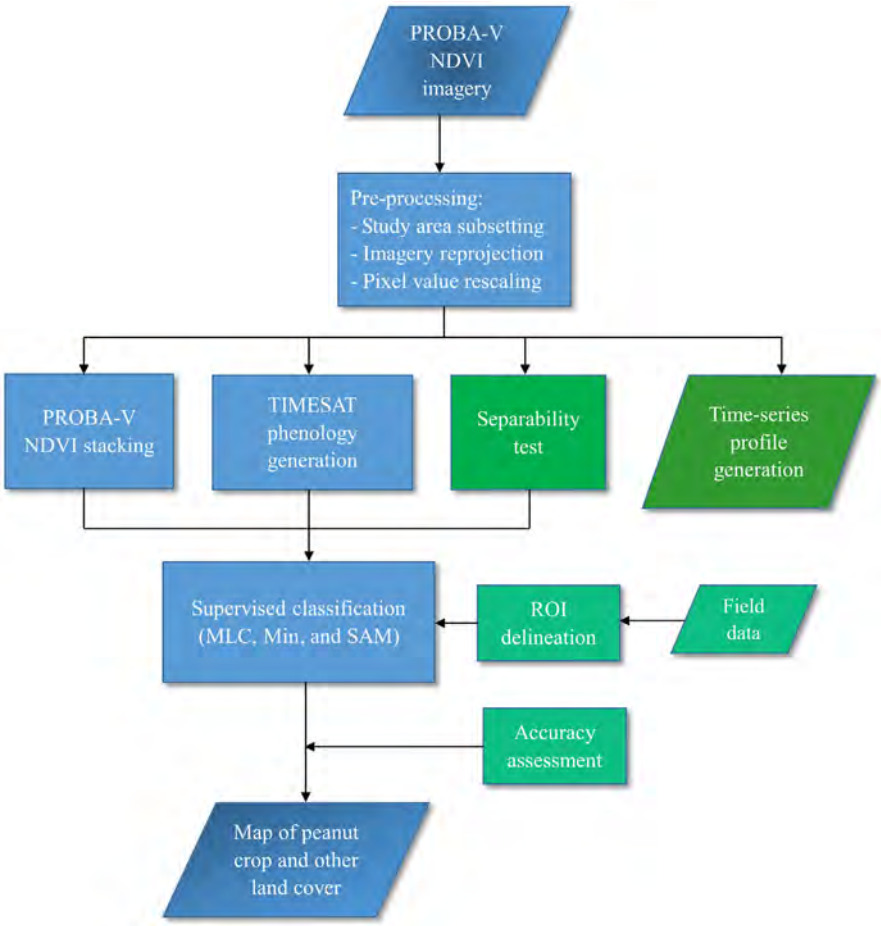

Fig. 3 Flowchart of data and key processing tasks employed in the study.

Downloaded From: https://www.spiedigitallibrary.org/journals/Journal-of-Applied-Remote-Sensing on 7/24/2018
Terms of Use: https://www.spiedigitallibrary.org/terms-of-use

Table 3 Eleven phenological parameters of the TIMESAT software program.

Phenological parameters	Label	Description
Start of the season	a	Similar to green-up period
End of the season	b	Harvesting period
Length of the season	c	Growing period
Base value	d	The average of minimum value of left and right of the season
Middle season	e	The mean value of the times, where the left edge has increased to the 80% level and the right edge has decreased to the 80% level
Maximum value	f	Phenology peak where time-series hit its highest data value
Seasonal amplitude	g	The difference between the maximum value and the base level
Left derivative (i.e., rate of increase at the beginning of the season)	—	The ratio of the difference between the left 20% and 80% levels of the fitted function
Right derivative (i.e., rate of decrease at the end of the season)	—	The absolute value of the ratio of the difference between the right 20% and 80% levels of the fitted function
Small integral	h	The area between start and end of the season, and between base value and maximum value
Large integral	h + i	The area under fitting curve, between start and end of the season

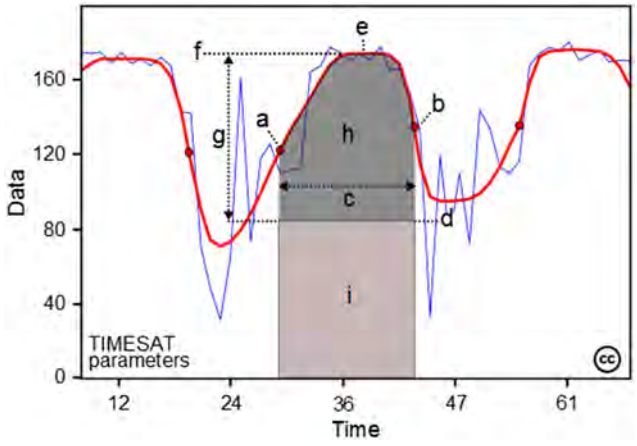

Fig. 4 Some of the phenological parameters generated from the TIMESAT program: (a) beginning of season, (b) end of season, (c) length of season, (d) base value, (e) time of middle of season, (f) maximum value, (g) amplitude, (h) small integrated value, and (h + i) large integrated value. The blue line represents the original time-series data, while the red line represents filtered data.[30]

the best-fitting method and fine-tuning the program parameter settings. The parameter settings for running the program in this study were summarized in Table 4.

2.6 *Image Classification and Accuracy Assessment*

Image classification techniques were performed for two datasets, i.e., stack of PROBA-V NDVI imagery and stack of phenological parameters of PROBA-V NDVI imagery derived from the

Downloaded From: https://www.spiedigitallibrary.org/journals/Journal-of-Applied-Remote-Sensing on 7/24/2018
Terms of Use: https://www.spiedigitallibrary.org/terms-of-use

Table 4 TIMESAT parameter settings used in this study.

Parameters	Value	Description
Amplitude value	0	0 = include all pixels in the processing
Spike method	1	To detect and remove outliners and spike
		1 = median filter method
Spike value	2	To determine the removing degree
		Low value will remove more spike and outliners
Seasonal parameter	0.5	To determine the number of season
		Value is between 0 and 1, where 0 = dual seasons and 1 = single season
Envelope iterations	3	3 = two additional fits
		Function fits to approach the upper envelope of time-series imagery
Adaptation strength	2	To indicate the strength of upper envelope adaptation. Value is a number between 1 and 10.
Start of season method	1	To determine start/end of the season
		1 = amplitude (start/end where the fitted curve reaches a proportion of seasonal amplitude)
Season start	0.2	The proportion of left minimum value
Season stop	0.2	The proportion of right minimum value

Table 5 Reference data division into training and test samples.

Samples	The number of pixels	Percentage (%)
Training	1221	72.25
Test	469	27.75
Total	1690	100

TIMESAT program. In this study, a supervised classification algorithm, i.e., maximum likelihood classification (MLC), was used to map peanut crops, other crops, and additional land cover classes using ENVI 5.0 software.[61] In previous studies, the classification accuracy produced from MLC was found to be comparable with machine learning algorithms, such as support vector machine and RF.[16,62,63] To compare the results gained by MLC, this study also used other supervised classification algorithms, namely minimum distance classification (Min) and spectral angle mapper (SAM). In MLC, an inadequate training pixel number can produce poor classification results, while the Min method can handle limited pixel counts. The reference data of 1690 pixels were divided into two groups, i.e., training and test samples (Table 5). The accuracy assessment of classification results was conducted using an error matrix to calculate the overall accuracy, kappa coefficient, producer accuracy (PA), and user accuracy (UA).[64]

3 Results

3.1 *Time-Series Profiles and Separability Test*

Time-series profiles characterized the reflectance pattern of each classified class, which then can be used to observe their differences. The mean value of PROBA-V NDVI time series during the

Downloaded From: https://www.spiedigitallibrary.org/journals/Journal-of-Applied-Remote-Sensing on 7/24/2018
Terms of Use: https://www.spiedigitallibrary.org/terms-of-use

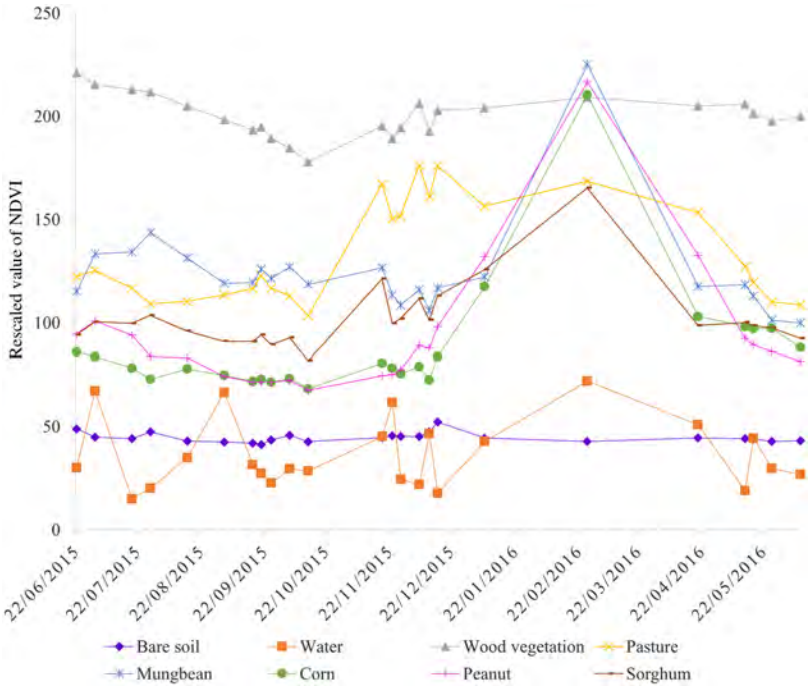

Fig. 5 Mean NDVI profiles of different crops and land cover classes extracted from PROBA-V NDVI time-series imagery.

period of June 22, 2015, to June 9, 2016 (Fig. 5) for each feature class showed distinct profiles, especially between crop and noncrop classes. Noncrop classes, i.e., woody vegetation, bare soil, water, and pasture, showed more even profiles, since these objects tend to be static throughout time. On the other hand, crop classes experienced a dynamic life-cycle growth, starting from planting, peak season, and senescence, which was then reflected in their time-series profiles. The crop profiles formed a curved shape, which started from a planting season, then increased until reaching a maximum reflectance value (peak), and finally decreased to a period of senescence where the crops were harvested. In addition, each crop grows in a specific period depending on its characteristics, climate, and water availability. As a result, different crops may have different or similar time-series profiles. In this study, mung bean and corn profiles were almost similar, with the difference apparent in planting time (start of the season). Mung bean was planted at the beginning of January 2016, whereas corn was planted in the middle of December 2015. The profile of peanut crops was slightly different from those two previously mentioned crops. Due to its longer growing period, i.e., 110 to 170 days (16 to 24 weeks),[2] peanut planting and harvesting (end of the season) times were totally different from other crops, i.e., November 2015 and May 2016, respectively. Among all crops, sorghum presented a different profile, with significant difference in its peak NDVI value, which was the lowest among others. The peak NDVI value for the other three crops was almost similar. The harvesting times for mung bean, sorghum, and corn were relatively similar; however, the NDVI value of mung bean was different from the other two crops. The figure also illustrated that during crop-growing seasons, there was a limited number of NDVI imagery. It was also observed that spectral responses outside of the crop growth period, i.e., June to October 2015, tend to be static, indicating that crops were not planted during this time.

Good separability of values among all classes was found for both the 24-layer PROBA-V NDVI imagery and the corresponding phenological parameters. The results of JM distance calculations between class pairs in PROBA-V NDVI imagery were dominated by 2.00 (Table 6), which is the highest measure of class separation. This is slightly better than JM distance in phenological parameters, in which two class pairs resulted in 1.88 JM (sorghum and pasture) and 1.92 JM (water and bare soil). The dominant JM distance for phenological parameters was 1.99 (Table 7).

Downloaded From: https://www.spiedigitallibrary.org/journals/Journal-of-Applied-Remote-Sensing on 7/24/2018
Terms of Use: https://www.spiedigitallibrary.org/terms-of-use

Table 6 Separability of time-series PROBA-V NDVI imagery.

Classes	Peanut	Corn	Mung bean	Sorghum	Woody vegetation	Pasture	Water	Bare soil
Peanut	—	1.99	2.00	1.99	2.00	1.99	2.00	2.00
Corn	1.99	—	2.00	1.99	2.00	1.99	2.00	2.00
Mung bean	2.00	2.00	—	2.00	2.00	1.99	2.00	2.00
Sorghum	1.99	1.99	2.00	—	2.00	1.99	2.00	2.00
Woody vegetation	2.00	2.00	2.00	2.00	—	1.99	2.00	2.00
Pasture	1.99	1.99	1.99	1.99	1.99	—	2.00	2.00
Water	2.00	2.00	2.00	2.00	2.00	2.00	—	2.00
Bare soil	2.00	2.00	2.00	2.00	2.00	2.00	2.00	—

Table 7 Separability of phenological parameters of PROBA-V NDVI.

Classes	Peanut	Corn	Mung bean	Sorghum	Woody vegetation	Pasture	Water	Bare soil
Peanut	—	1.99	1.99	1.99	2.00	1.99	1.99	2.00
Corn	1.99	—	1.99	1.99	1.99	1.99	1.98	1.99
Mung bean	1.99	1.99	—	1.98	1.99	1.99	1.99	1.99
Sorghum	1.99	1.99	1.98	—	1.99	1.88	1.98	1.99
Woody vegetation	2.00	1.99	1.99	1.99	—	1.99	1.99	1.99
Pasture	1.99	1.99	1.99	1.88	1.99	—	1.99	2.00
Water	1.99	1.98	1.99	1.98	1.99	1.99	—	1.92
Bare soil	2.00	1.99	1.99	1.99	1.99	2.00	1.92	—

3.2 *TIMESAT Features*

Time-series profiles resulting from image data processing using the TIMESAT program also showed distinctive profiles between crop and noncrop classes (Fig. 6). The profiles were selected from a sample pixel of each class, which in general represent the group pixel values. Since TIMESAT requires at least three years of time-series data (as previously indicated), one-year time-series data of 24 imagery employed in this study were replicated into 72 imagery (the axis in the profiles) as recommended by the software. However, the analysis in this study only focused on the original time-series data, i.e., the center data, from 25 to 48.

In the time-series profiles from TIMESAT, noncrop classes showed generally constant NDVI values. Bare soil and water had low NDVI values (around 35 and 50, respectively), while pasture and woody vegetation had high NDVI value (around 135 and 210, respectively). Profiles of four crop classes (i.e., peanut, corn, sorghum, and mung bean) represent its phenological phases, which depict the start, peak, and end of seasons. Among all crop classes, peanut showed the longest growing period, while the other three crops presented almost similar length of growing period.

In the second phase of analysis, the phenological parameters output of PROBA-V NDVI imagery resulted from the TIMESAT program was used to map peanut crops. To achieve higher classification accuracy, imagery layers with small discrimination information for class separability were avoided by carrying out dataset dimensionality reduction.[56] Thus, in this study, only parameters that had most useful information to separate eight classified classes were selected. Two out of 11 phenological parameters, i.e., "maximum value" and "season start," failed in

Downloaded From: https://www.spiedigitallibrary.org/journals/Journal-of-Applied-Remote-Sensing on 7/24/2018
Terms of Use: https://www.spiedigitallibrary.org/terms-of-use

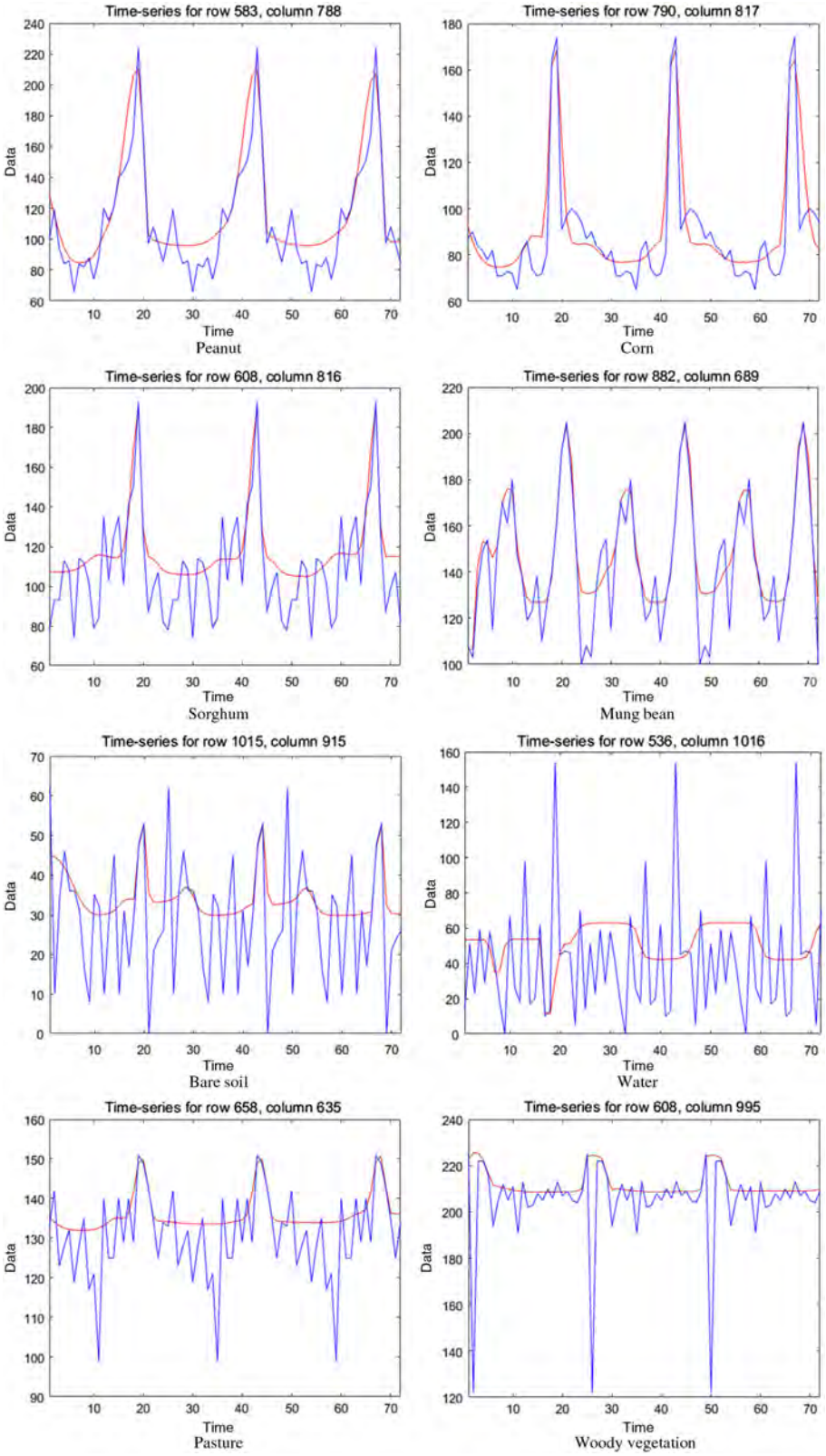

Fig. 6 Time-series profiles from the TIMESAT program: blue line represents original time-series data, while the red line represents fitted time-series data using asymmetric Gaussian method.

Downloaded From: https://www.spiedigitallibrary.org/journals/Journal-of-Applied-Remote-Sensing on 7/24/2018
Terms of Use: https://www.spiedigitallibrary.org/terms-of-use

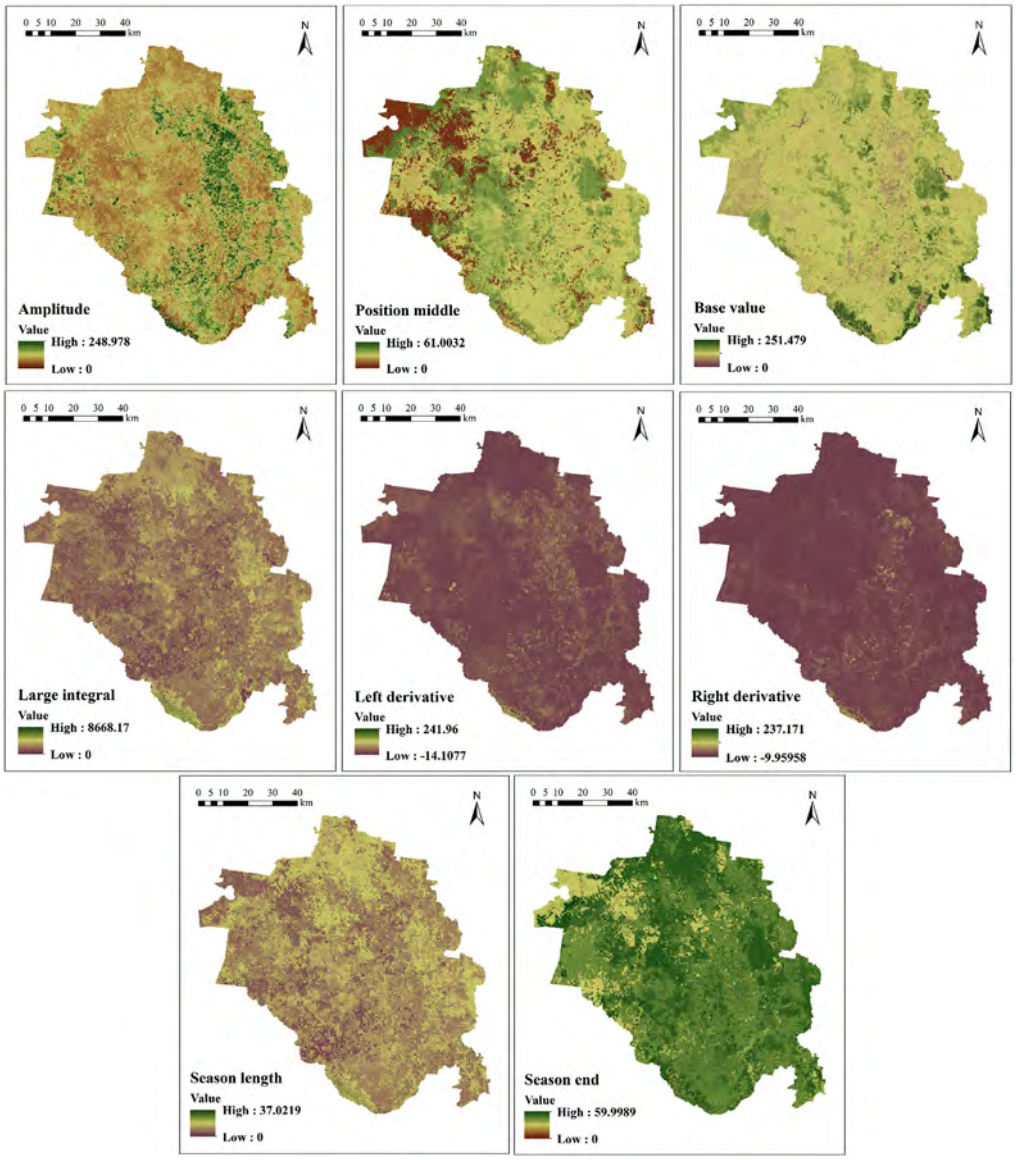

Fig. 7 Phenological parameters used in mapping peanut crops and other crop/land cover classes.

performing the separability test, while including the "small integral" parameter has reduced the classification accuracy. Therefore, only eight phenological parameters were used in the classification process, namely amplitude, position middle, base value, large integral, left derivative, right derivative, season end, and season length (Fig. 7).

3.3 *Classification Result*

The classification results of MLC, Min, and SAM for both PROBA-V NDVI imagery and its phenological parameters derived from the TIMESAT program are shown in Fig. 8. In conducting classifications, the process involved choosing the most suitable parameter for each classification algorithm to achieve the best and the most appropriate classified imagery. Visual analysis through comparison of different land cover classes, i.e., woody vegetation, water, bare soil, and pasture, in classified imagery and Landsat 8 imagery showed similar distribution. Classification results of the MLC algorithm for both NDVI and phenological parameters showed better outcomes than Min and SAM classifier, even though parameter adjustment of these two latter classifiers had been repeatedly tested several times.

Downloaded From: https://www.spiedigitallibrary.org/journals/Journal-of-Applied-Remote-Sensing on 7/24/2018
Terms of Use: https://www.spiedigitallibrary.org/terms-of-use

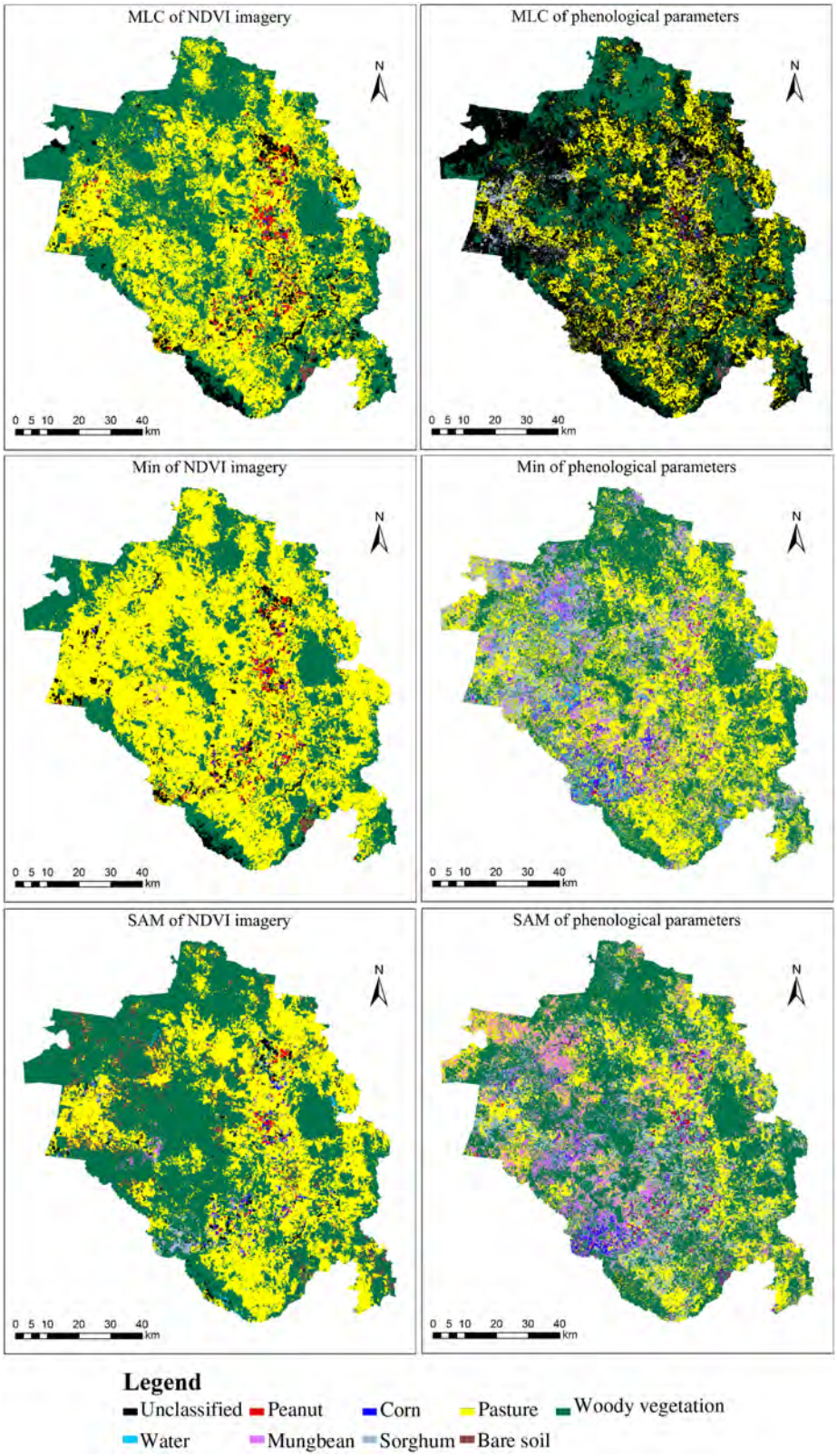

Fig. 8 Classified image outputs from MLC, Min, and SAM classifiers (the unclassified pixels occurred due to the threshold values applied in MLC).

Downloaded From: https://www.spiedigitallibrary.org/journals/Journal-of-Applied-Remote-Sensing on 7/24/2018
Terms of Use: https://www.spiedigitallibrary.org/terms-of-use

3.4 *Accuracy Assessment*

The classification performance was analyzed based on error matrix and kappa coefficient (k) value for the three classification methods, i.e., MLC, Min, and SAM, for both phenological parameters and NDVI imagery. In general, NDVI imagery provided better classification performance than phenological parameters for all classification methods (Table 8). Comparing the three classification methods, MLC was the best classification method in this study, for both phenological parameters and NDVI imagery. Looking in closer detail, the overall accuracy of the MLC classifier for the NDVI imagery was the highest, i.e., 92.75%, compared to 79.53% of the MLC classifier for the phenological parameters. The lowest overall accuracy was 62.26%, which resulted from the Min classifier of phenological parameters. The kappa coefficients (k) for NDVI imagery classification varied between 0.73 and 0.9, which is considered to be very good ($0.61 < k \leq 0.80$) and excellent ($k > 0.81$).[65] On the other hand, the k values for phenological parameters classification were 0.55 to 0.76, which can be considered as moderate ($0.41 < k \leq 0.60$) and very good.[65]

Table 8 Overall accuracy and Kappa coefficient of classified images.

	NDVI imagery		Phenological parameters	
Classification	Overall accuracy (%)	Kappa coefficient	Overall accuracy (%)	Kappa coefficient
MLC	92.75	0.91	79.53	0.76
Min	85.29	0.82	62.26	0.55
SAM	77.83	0.73	66.74	0.60

Table 9 Classic contingency matrix of NDVI imagery dataset.

Reference test data (number of pixels)										
	Peanut	Corn	Mung bean	Sorghum	Woody vegetation	Pasture	Water	Bare soil	Total	UA (%)
MLC of NDVI										
Peanut	52	10	0	0	0	0	0	0	62	83.87
Corn	0	41	0	0	0	0	0	0	41	100
Mung bean	0	0	16	0	0	0	0	0	16	100
Sorghum	0	0	0	12	0	2	0	0	14	85.71
Woody vegetation	0	0	0	1	129	0	0	0	130	99.23
Pasture	0	0	0	0	0	95	0	0	95	100
Water	0	0	0	0	0	0	48	0	48	100
Bare soil	0	0	0	0	0	0	0	42	42	100
Unclassified	14	0	1	0	6	0	0	0	21	—
Total	66	51	17	13	135	97	48	42	469	—
PA (%)	78.79	80.39	94.12	92.31	95.56	97.94	100	100	—	—
Overall accuracy = 92.75% and kappa coefficient = 0.91										

Downloaded From: https://www.spiedigitallibrary.org/journals/Journal-of-Applied-Remote-Sensing on 7/24/2018
Terms of Use: https://www.spiedigitallibrary.org/terms-of-use

Table 9 (*Continued*).

Reference test data (number of pixels)										
	Peanut	Corn	Mung bean	Sorghum	Woody vegetation	Pasture	Water	Bare soil	Total	UA (%)
SAM of NDVI										
Peanut	51	0	0	0	0	0	0	0	51	100
Corn	1	51	3	5	0	0	0	0	60	85
Mung bean	0	0	8	0	0	0	0	0	8	100
Sorghum	0	0	2	5	0	8	0	0	15	33.33
Woody vegetation	0	0	1	0	128	19	0	30	178	71.91
Pasture	0	0	0	3	1	70	0	0	74	94.59
Water	4	0	1	0	0	0	41	0	46	89.13
Bare soil	0	0	0	0	6	0	0	11	17	64.71
Unclassified	10	0	2	0	0	0	7	1	20	—
Total	66	51	17	13	135	97	48	42	469	—
PA (%)	77.27	100	47.06	38.46	94.81	72.16	85.42	26.19	—	—
Overall accuracy = 77.83% and kappa coefficient = 0.73										
Min of NDVI										
Peanut	39	1	0	2	0	0	0	0	42	92.86
Corn	13	50	0	1	0	0	0	0	64	78.13
Mung bean	0	0	1	0	0	0	0	0	1	100
Sorghum	0	0	0	3	0	0	0	0	3	100
Woody vegetation	0	0	3	0	121	0	0	0	124	97.58
Pasture	0	0	4	3	8	97	0	0	112	86.61
Water	0	0	0	0	0	0	48	1	49	97.96
Bare soil	0	0	0	0	0	0	0	41	41	100
Unclassified	14	0	9	4	6	0	0	0	33	—
Total	66	51	17	13	135	97	48	42	469	—
PA (%)	59.09	98.04	5.88	23.08	89.63	100	100	97.62	—	—
Overall accuracy = 85.29% and kappa coefficient = 0.82										

The PA and UA of the image classified using MLC of NDVI imagery presented the best result, i.e., ≥78% (Table 9), which indicated a good classification performance. The MLC of phenological parameters also gave a good result for the PA and UA, except for the mung bean class which had PA of 52%, indicating that many pixels belonging to this class were

Downloaded From: https://www.spiedigitallibrary.org/journals/Journal-of-Applied-Remote-Sensing on 7/24/2018
Terms of Use: https://www.spiedigitallibrary.org/terms-of-use

omitted. Compared to phenological parameters, the SAM of NDVI imagery provided better results, where the UA was slightly better than PA. On the other hand, the application of Min in phenological parameters resulted in low PA and UA, which indicated the high inclusion (omission error) and exclusion (commission error) of pixels to the targeted class. In relation to the peanut class, all classification methods gave good results in PA and UA for both the NDVI imagery and the phenological parameters, i.e., >75%, except for PA of the Min algorithm which accounted for 59%. Interestingly, the SAM algorithm provided the best result in the peanut class for UA of NDVI imagery and PA of phenological parameters, i.e., 100% and 90%, respectively. However, the MLC algorithm still presented the best results for PA of NDVI imagery and UA of phenological parameters, i.e., 79% and 88%, respectively.

4 Discussion

Our study demonstrates the ability of using imagery from a recent satellite mission, PROBA-V, in mapping the peanut cropping area in the South Burnett region of Queensland, Australia. It successfully differentiated and mapped eight classes of crops and other land cover features using time-series PROBA-V NDVI 100-m imagery and its phenological parameters. The good performance of PROBA-V data could be attributed to its improvement in spatial resolution compared to traditional time-series data, such as the commonly used MODIS 250-m data. The choice of 100-m spatial resolution contributed to desirable outcomes of this study, as Roumenina et al.[66] found that PROBA-V 100 m achieved better results than PROBA-V 300 m in mapping crops in Bulgaria. In addition, the compact design of PROBA-V platform and payload, which is equipped with vegetation sensors, enables the application of high-performance operation to achieve its specific objective in providing time-series vegetation data.[52]

The PROBA-V NDVI mean time-series profiles in this study indicated that this satellite sensor has successfully captured temporal separability between eight crops and other land cover classes examined. In addition, it showed the ability of PROBA-V NDVI time series in presenting phenological stages of crop classes included in this study. This time-series imagery was also analyzed further using the TIMESAT program which smoothed the time-series data and generated phenological parameter maps. It was found that the phenology profiles of eight classes from the TIMESAT program closely resemble the mean NDVI time-series profiles.

Comparing two datasets, i.e., PROBA-V NDVI imagery and its phenological parameters derived from the TIMESAT program, the former produced better overall accuracy in all classification methods. However, not all phenological parameters were included in the classification efforts. Phenological parameters of "maximum value" and "season start" failed in the separability test, while including the "small integral" parameter in the classification has decreased the classification accuracy. It was suggested that the limited number of NDVI imagery during the crop growth period, especially in the peak of the season, has contributed to the exclusion of these three parameters. Moreover, the better outcomes from the separability test of JM distance in NDVI imagery (dominated by 2.00) than the phenological parameters (dominated by 1.99) have predicted the better accuracy results of NDVI imagery. Additionally, in a study of crop mapping in Bulgaria, it was sufficient to utilize only three to four PROBA-V imageries distributed along the crop growth period, to acquire good classification accuracy.[66] Since this study used 24 stacked imagery of the PROBA-V NDVI dataset, it would be expected that this number was more than enough to achieve good classification results. It should be noted that the ROI development for classification and accuracy assessment was performed in the phenological parameters stack. This study recognizes that the distinct spectral differences between classes in the phenological parameters stack, compared to NDVI imagery, were useful in guiding and locating ROIs. Different results could be generated from this study if the phenological parameters stack was not used in determining ROI. In this case, it would be expected that if NDVI imagery was used to locate ROI, different ROI datasets would take place.

The MLC algorithm performed better than the SAM and the Min, with an accuracy of 92.75%. This result agrees with Beyer et al.[16] in evaluating eight classification algorithms

Downloaded From: https://www.spiedigitallibrary.org/journals/Journal-of-Applied-Remote-Sensing on 7/24/2018
Terms of Use: https://www.spiedigitallibrary.org/terms-of-use

(including MLC, SAM, and Min) to map agricultural crops in Israel, which resulted in the superior performance of MLC compared to most of the classification algorithms. A comparison of the three classification algorithms (i.e., MLC, SAM, and Min) was also carried out by Fontanelli et al.[67] in mapping crops in Italy, which found MLC to be the best algorithm. Moreover, the classification accuracy achieved in this work was comparable to the accuracy results of previous crop mapping studies using PROBA-V imagery. Lambert et al.[45] mapped crops in the Sahelian and Sudan region using PROBA-V 100 m and attained an accuracy of 84%. High accuracy between 65% and 86% was also achieved in using this satellite data to map crops globally in Belgium, Russia, Ukraine, and Brazil.[44] Furthermore, PROBA-V data have been successfully used to map crops with similar phenology profiles (i.e., corn and soybean) in China with accuracy of 73.29%.[39] It is important to realize that even though the number of classes used in our study was relatively large, i.e., eight classes in total, the application of MLC in NDVI imagery produced very good overall accuracy with PA and UA of each class ≥78%. Interestingly, this result was achieved without masking out noncropping areas (e.g., using land use maps), which could further improve the accuracy, as achieved by Potgieter et al.[24] Conversely, masking out land use cover could also generate some problems related to the currency of data and accuracy of land use map employed.

Peanut crop maps resulting from this study will be valuable in supporting peanut production, yield prediction, and commodity forecasting, especially as focused work on peanut crop mapping is limited. Combining with yield per unit area, an estimation of peanut production can be calculated, which then can be used to support decisions for planning and management purposes. Moreover, this study utilized remote-sensing technology that could overcome significant shortcomings of traditional survey methods. The use of multiband data, such as vegetation indices, and time-series imagery as employed in this study has offered great benefits in peanut crop mapping.

5 Conclusion

The use of imagery from a recently launched satellite, PROBA-V, was successful in mapping peanut crops in the South Burnett region in Queensland, Australia, using two datasets, i.e., PROBA-V 100-m NDVI imagery and its derived phenological parameters. In general, the overall accuracy of NDVI imagery outweighs phenological parameters, but specifically for peanut crops, both datasets have performed very well. The best classification method for both datasets involving all classes was the MLC approach, i.e., 92.75% for NDVI imagery and 79.53% for phenological parameters. However, in classifying peanut crops, all classification methods performed well for PA and UA, with the best results provided by MLC and SAM classifiers. It is recommended that sufficient number of imagery during the crop growth period is available to enable modeling of phenological parameters. Furthermore, the use of machine learning algorithms has not been considered in this study but can be explored in further work. To the best of our knowledge, this is the first study that used PROBA-V imagery in crop mapping in Australia. Our study confirmed that the PROBA-V satellite has great potential in crop area mapping and can fulfill its mission to support vegetation-user communities. The findings in this study reinforce the necessity to continue the PROBA-V mission, which was originally designed as a "gap-filler mission," by launching its second-generation satellite.

Disclosures

The authors declare that there are no conflicts of interest.

Acknowledgments

We would like to thank the Australian Government for the Australia Awards Scholarship awarded to the first author. We would also like to acknowledge the valuable comments and suggestions from our colleague Thong Huy Nguyen and the helpful proofreading work from Dr. Barbara Harmes.

Downloaded From: https://www.spiedigitallibrary.org/journals/Journal-of-Applied-Remote-Sensing on 7/24/2018
Terms of Use: https://www.spiedigitallibrary.org/terms-of-use

References

1. M. Adomou et al., "Disease assessment methods and their use in simulating growth and yield of peanut crops affected by leafspot disease," *Ann. Appl. Biol.* **146**(4), 469–479 (2005).
2. DPIF, *Best Management Practices Peanuts*, Department of Primary Industries and Fisheries, The State of Queensland, Queensland (2007).
3. G. Wright, L. Wieck, and D. O'Connor, *Peanut Production Guide*, Peanut Company of Australia, Kingaroy, Australia (2017).
4. QGSO, "Queensland Statistics: Queensland Government Statistician's Office," 2016, http://www.qgso.qld.gov.au/products/tables/agriculture-gross-value-production/index.php (30 May 2016).
5. J. Gallego et al., *Best Practices for Crop Area Estimation with Remote Sensing*, Joint Research Center, Ispra (2008).
6. M. Craig and D. Atkinson, "A literature review of crop area estimation: FAO," 2013 http://www.fao.org/search/en/?cx=018170620143701104933%3Aqq82jsfba7w&q=www.fao.org%2F...%2FCrop_Area_Estimation_Lit_review&cof=FORID%3A9 (25 March 2017).
7. T. Iizumi and N. Ramankutty, "How do weather and climate influence cropping area and intensity?" *Global Food Secur.* **4**, 46–50 (2015).
8. M. K. Srivastava, *Crop Monitoring for Improved Food Security*, FAO and ADB, Bangkok (2015).
9. A. Robson, G. Wright, and S. Phinn, "Remote sensing applications in peanuts: the assessment of crop maturity, yield, disease, irrigation efficiency and best management practices using temporal images," in *5th Australian Controlled Traffic Farming & Precision Agriculture Conf.*, Australian Controlled Traffic Farming Association Inc (ACTFA), Perth (2007).
10. B. Schultz et al., "Self-guided segmentation and classification of multi-temporal Landsat 8 images for crop type mapping in southeastern Brazil," *Remote Sens.* **7**(11), 14482–14508 (2015).
11. A. Knudby, "An AVHRR-based model of groundnut yields in the peanut basin of Senegal," *Int. J. Remote Sens.* **25**(16), 3161–3175 (2004).
12. J. Im and J. R. Jensen, "Hyperspectral remote sensing of vegetation," *Geogr. Compass* **2**(6), 1943–1961 (2008).
13. M. L. Whiting et al., "Hyperspectral mapping of crop and soils for precision agriculture," *Proc. SPIE* **6298**, 62980B (2006).
14. I. Vorovencii, "The hyperspectral sensors used in satellite and aerial remote sensing," *Bulletin of the Transilvania University of Brasov*, Series II, Forestry, Wood Industry, Agriculture, and Food Engineering, Vol. **2**, 51–56 (2009).
15. U. Alganci et al., "Parcel-level identification of crop types using different classification algorithms and multi-resolution imagery in southeastern turkey," *Photogramm. Eng. Remote Sens.* **79**(11), 1053–1065 (2013).
16. F. Beyer et al., Eds., "Improved crop classification using multitemporal RapidEye data," in *8th Int. Workshop on the Analysis of Multitemporal Remote Sensing Images (Multi-Temp)*, IEEE (2015).
17. C. Gómez, J. C. White, and M. A. Wulder, "Optical remotely sensed time series data for land cover classification: a review," *ISPRS J. Photogramm. Remote Sens.* **116**, 55–72 (2016).
18. F. Gao et al., "Toward mapping crop progress at field scales through fusion of Landsat and MODIS imagery," *Remote Sens. Environ.* **188**, 9–25 (2017).
19. B. D. Wardlow, S. L. Egbert, and J. H. Kastens, "Analysis of time-series MODIS 250 m vegetation index data for crop classification in the US Central Great Plains," *Remote Sens. Environ.* **108**(3), 290–310 (2007).
20. P. M. Atkinson et al., "Inter-comparison of four models for smoothing satellite sensor time-series data to estimate vegetation phenology," *Remote Sens. Environ.* **123**, 400–417 (2012).
21. C. Atzberger, "Advances in remote sensing of agriculture: context description, existing operational monitoring systems and major information needs," *Remote Sens.* **5**(2), 949–981 (2013).

Downloaded From: https://www.spiedigitallibrary.org/journals/Journal-of-Applied-Remote-Sensing on 7/24/2018
Terms of Use: https://www.spiedigitallibrary.org/terms-of-use

22. Y. Hirosawa, S. E. Marsh, and D. H. Kliman, "Application of standardized principal component analysis to land-cover characterization using multitemporal AVHRR data," *Remote Sens. Environ.* **58**(3), 267–281 (1996).
23. M. E. Jakubauskas, D. R. Legates, and J. H. Kastens, "Harmonic analysis of time-series AVHRR NDVI data," *Photogramm. Eng. Remote sens.* **67**(4), 461–470 (2001).
24. A. B. Potgieter et al., "Estimating crop area using seasonal time series of enhanced vegetation index from MODIS satellite imagery," *Crop Pasture Sci.* **58**(4), 316–325 (2007).
25. J. Chen et al., "A simple method for reconstructing a high-quality NDVI time-series data set based on the Savitzky–Golay filter," *Remote Sens. Environ.* **91**(3), 332–344 (2004).
26. X. Zhang et al., "Monitoring vegetation phenology using MODIS," *Remote Sens. Environ.* **84**(3), 471–475 (2003).
27. P. Jönsson and L. Eklundh "Seasonality extraction by function fitting to time-series of satellite sensor data," *IEEE Trans. Geosci. Remote Sens.* **40**(8), 1824–1832 (2002).
28. M. Foerster et al., Eds., "TimeSpec—a software tool for analyzing time-series of spectral data," in *IEEE Int. Geoscience and Remote Sensing Symp. (IGARSS)*, IEEE (2014).
29. P. Jönsson and L. Eklundh, "TIMESAT—a program for analyzing time-series of satellite sensor data," *Comput. Geosci.* **30**(8), 833–845 (2004).
30. L. Eklundh and P. Jönsson, *TIMESAT 3.2 with Parallel Processing—Software Manual*, Lund University and Malmo University (2015).
31. S. Yang et al., Eds., "Mapping rice paddy in Henan Province using multi-temporal MODIS images," in *Int. Conf. on Remote Sensing, Environment and Transportation Engineering (RSETE)*, IEEE (2011).
32. K. Hentze, F. Thonfeld, and G. Menz, "Evaluating crop area mapping from MODIS time-series as an assessment tool for Zimbabwe's Fast Track Land Reform Programme," *PLoS One* **11**(6), e0156630 (2016).
33. H. Sun et al., "Winter wheat mapping using temporal signatures of MODIS vegetation index data," *Int. J. Remote Sens.* **33**(16), 5026–5042 (2012).
34. K. Navulur, *Multispectral Image Analysis Using the Object-Oriented Paradigm*, CRC Press Taylor & Francis Group, Boca Raton, Florida (2006).
35. A. Khan et al., "Landsat-based wheat mapping in the heterogeneous cropping system of Punjab, Pakistan," *Int. J. Remote Sens.* **37**(6), 1391–1410 (2016).
36. F. Petitjean, J. Inglada, and P. Gancarski, "Assessing the quality of temporal high-resolution classifications with low-resolution satellite image time series," *Int. J. Remote Sens.* **35**(7), 2693–2712 (2014).
37. Y. Xie, Z. Sha, and M. Yu, "Remote sensing imagery in vegetation mapping: a review," *J. Plant Ecol.* **1**(1), 9–23 (2008).
38. Z. Pan et al., "Mapping crop phenology using NDVI time-series derived from HJ-1 A/B data," *Int. J. Appl. Earth Obs. Geoinf.* **34**, 188–197 (2015).
39. X. Zhang et al., "Crop mapping using PROBA-V time series data at the Yucheng and Hongxing Farm in China," *Remote Sens.* **8**(11), 915 (2016).
40. M. Ozdogan and C. E. Woodcock, "Resolution dependent errors in remote sensing of cultivated areas," *Remote Sens. Environ.* **103**(2), 203–217 (2006).
41. M. W. Liu, M. Ozdogan, and X. Zhu, "Crop type classification by simultaneous use of satellite images of different resolutions," *IEEE Trans. Geosci. Remote Sens.* **52**(6), 3637–3649 (2014).
42. E. Wolters et al., "PROBA-V product user manual version: 2.1," VITO (2017).
43. Z. Mingwei et al., "Crop discrimination in Northern China with double cropping systems using Fourier analysis of time-series MODIS data," *Int. J. Appl. Earth Obs. Geoinf.* **10**(4), 476–485 (2008).
44. Y. Ö. Durgun et al., "Crop area mapping using 100-m Proba-V time series," *Remote Sens.* **8**(7), 585 (2016).
45. M.-J. Lambert, F. Waldner, and P. Defourny, "Cropland mapping over Sahelian and Sudanian agrosystems: a knowledge-based approach using PROBA-V time series at 100-m," *Remote Sens.* **8**(3), 232 (2016).

Downloaded From: https://www.spiedigitallibrary.org/journals/Journal-of-Applied-Remote-Sensing on 7/24/2018
Terms of Use: https://www.spiedigitallibrary.org/terms-of-use

46. ABS, "National Regional Profile (NRP): South Burnett: ABS," 15 April 2016, http://stat.abs.gov.au/itt/r.jsp?RegionSummary&region=36630&dataset=ABS_REGIONAL_LGA&geoconcept=REGION&datasetASGS=ABS_REGIONAL_ASGS&datasetLGA=ABS_REGIONAL_LGA&regionLGA=REGION&regionASGS=REGION (31 March 2017).
47. BoM, "Climate classifications BoM," 2016, http://www.bom.gov.au/jsp/ncc/climate_averages/climate-classifications/index.jsp?maptype=seasgrpb#maps (17 April 2017).
48. South Burnett Regional Council, "South Burnett economic brief," SBR Council (2014).
49. P. Sorby and R. E. Reid, *Soils and Agricultural Suitability of the South Burnett Agricultural Lands, Queensland*, Department of Natural Resources and Mines, Brisbane (2001).
50. South Burnett Regional Council, "South Burnett Regional Council 2014–15 annual report," SBR Council (2016).
51. DAF, "Broadacre field crops: DAF," 13 October 2014, https://www.daf.qld.gov.au/plants/field-crops-and-pastures/broadacre-field-crops (6 March 2017).
52. M. Francois et al., "The PROBA-V mission: the space segment," *Int. J. Remote Sens.* **35**(7), 2548–2564 (2014).
53. VITO, "Proba Vegetation the small satellite for global vegetation monitoring Belgium: VITO," 2016, http://proba-v.vgt.vito.be/ (24 April 2017).
54. K. Jia et al., "Land cover classification of Landsat data with phenological features extracted from time series MODIS NDVI data," *Remote Sens.* **6**(11), 11518–11532 (2014).
55. C. H. W. de Souza et al., "Mapping and discrimination of soya bean and corn crops using spectro-temporal profiles of vegetation indices," *Int. J. Remote Sens.* **36**(7), 1809–1824 (2015).
56. D. Arvor et al., "Classification of MODIS EVI time series for crop mapping in the state of Mato Grosso, Brazil," *Int. J. Remote Sens.* **32**(22), 7847–7871 (2011).
57. J. A. Richards, *Remote Sensing Digital Image Analysis: An Introduction*, Vol. **XXV**, 4th ed., 439 p., Springer, New York (2006).
58. Y. M. Gambarova et al., "Remote sensing and GIS as an advance space technologies for rare vegetation monitoring in Gobustan State National Park, Azerbaijan," *J. Geogr. Inf. Sys.* **2**(02), 93–99 (2010).
59. W. Jayawardhana and V. Chathurange, "Extraction of agricultural phenological parameters of Sri Lanka using MODIS, NDVI time series data," *Procedia Food Sci.* **6**, 235–241 (2016).
60. P. Jönsson and L. Eklundh, "Timesat: a software package to analyse time-series of satellite sensor data," 28 April 2015, http://web.nateko.lu.se/timesat/timesat.asp?cat=0 (16 March 2017).
61. Exelis Visual Information Solutions, *ENVI Version 5.0*, Exelis Visual Information Solutions, Boulder, Colorado (2012).
62. J. R. Otukei and T. Blaschke, "Land cover change assessment using decision trees, support vector machines and maximum likelihood classification algorithms," *Int. J. Appl. Earth Obs. Geoinf.* **12**, S27–S31 (2010).
63. F. Beyer, T. Jarmer, and B. Siegman, "Identification of agricultural crop types in Northern Israel using multitemporal rapid eye data," *Photogrammetrie-Fernerkundung-Geoinf.* **2015**(1), 21–32 (2015).
64. R. G. Congalton, "A review of assessing the accuracy of classifications of remotely sensed data," *Remote Sens. Environ.* **37**(1), 35–46 (1991).
65. J. R. Landis and G. G. Koch, "The measurement of observer agreement for categorical data," *Biometrics* **33**(1), 159–174 (1977).
66. E. Roumenina et al., "Single-and multi-date crop identification using PROBA-V 100 and 300 m S1 products on Zlatia test site, Bulgaria," *Remote Sens.* **7**(10), 13843–13862 (2015).
67. G. Fontanelli et al., Eds., "Agricultural crop mapping using optical and SAR multi-temporal seasonal data: a case study in Lombardy region, Italy," in *IEEE Int. Geoscience and Remote Sensing Symp. (IGARSS)*, IEEE (2014).

Haerani Haerani is currently a PhD student at the University of Southern Queensland (USQ) and a lecturer in the Department of Agricultural Engineering, Universitas Hasanuddin. She received her bachelor's degree in agricultural engineering from Universitas Hasanuddin in

Downloaded From: https://www.spiedigitallibrary.org/journals/Journal-of-Applied-Remote-Sensing on 7/24/2018
Terms of Use: https://www.spiedigitallibrary.org/terms-of-use

2002 and her master of science degree in engineering project management from the University of Melbourne in 2006. Her research interests include remote sensing and geospatial analyses in agriculture. She is a member of Indonesian Agricultural Engineering Association.

Armando Apan is a professor at the School of Civil Engineering and Surveying, USQ, Australia. He received his BSc (forestry) degree from the University of the Philippines, his MSc (natural resources) degree from the Asian Institute of Technology, Thailand, and his PhD (geography and environmental science) from Monash University, Australia. His research interests focus on the use of remote sensing and GIS in ecology, forestry, agriculture, and environmental management.

Badri Basnet is a lecturer at the USQ, where he is involved in teaching geographic information systems (GIS) and related courses (e.g., precision and smart technologies in agriculture, problem solving, etc.). He has extensive involvement in scholarship in learning and teaching (L&T) GIS at higher education institutions. His L&T research focus is in the development and use of open educational resources in GIS education.

Downloaded From: https://www.spiedigitallibrary.org/journals/Journal-of-Applied-Remote-Sensing on 7/24/2018
Terms of Use: https://www.spiedigitallibrary.org/terms-of-use